JOURNAL OF GEOPHYSICAL RESEARCH, VOL. 105, NO. E2, PAGES 4245–4262, FEBRUARY 25, 2000

Compositional analyses of small lunar pyroclastic deposits using Clementine multispectral data

Lisa R. Gaddis,[1] B. Ray Hawke,[2] Mark S. Robinson,[3] and Cassandra Coombs[4]

Abstract. Clementine ultraviolet-visible (UVVIS) data are used to examine the compositions of 18 pyroclastic deposits (15 small, three large) at 13 sites on the Moon. Compositional variations among pyroclastic deposits largely result from differing amounts of new basaltic (or juvenile) material and reworked local material entrained in their ejecta upon eruption. Characterization of pyroclastic deposit compositions allows us to understand the mechanisms of lunar explosive volcanism. Evidence for compositional differences between small pyroclastic deposits at a single site is observed at Atlas crater. At all sites, compositional variation among the small pyroclastic deposits is consistent with earlier classification based on Earth-based spectra: three compositional groups can be observed, and the trend of increasing mafic absorption band strength from Group 1 to Group 2 to Group 3 is noted. As redefined here, Group 1 deposits include those of Alphonsus West, Alphonsus Southeast, Alphonsus Northeast 2, Atlas South, Crüger, Franklin, Grimaldi, Lavoisier, Oppenheimer, Orientale, and Riccioli. Group 1 deposits resemble lunar highlands, with weak mafic bands and relatively high UV/VIS ratios. Group 2 deposits include those of Alphonsus Northeast 1, Atlas North, Eastern Frigoris East and West, and Aristarchus Plateau; Group 2 deposits are similar to mature lunar maria, with moderate mafic band depths and intermediate UV/VIS ratios. The single Group 3 deposit, J. Herschel, has a relatively strong mafic band and a low UV/VIS ratio, and olivine is a likely juvenile component. Two of the deposits in these groups, Orientale and Aristarchus, are large pyroclastic deposits. The third large pyroclastic deposit, Apollo 17/Taurus Littrow, has a very weak mafic band and a high UV/VIS ratio and it does not belong to any of the compositional groups for small pyroclastic deposits. The observed compositional variations indicate that highland and mare materials are also present in many large and small pyroclastic deposits, and they suggest that volcanic glasses or spheres may not be dominant juvenile components in all large pyroclastic deposits.

1. Introduction

Lunar pyroclastic deposits are volatile and metallic element (Fe and Ti) enriched remnants of ancient volcanic eruptions on the Moon, and they provide clues to conditions in the early lunar interior [e.g., *Papike et al.*, 1998] and to the distribution of potential resource materials for future exploitation [*Hawke et al.*, 1990]. Studies of lunar pyroclastic materials, especially the primary or juvenile picritic glasses, provide unique information on the composition of the mantle [e.g., *Delano*, 1986] and on the nature and origin of associated volatile elements in an otherwise volatile-depleted environment [e.g., *Heiken et al.*, 1974]. Possible fundamental differences between picritic glasses and mare basalts [e.g., lesser fractional crystallization and greater depth of origin for glasses; *Shearer and Papike*, 1993; *Papike et al.*, 1998] support their identification as the best examples of primitive materials on the Moon and attest to their importance in characterizing the lunar interior and as a starting place for understanding the origin and evolution of basaltic magmatism on the Moon. Remote-sensing analyses of these deposits have helped us to identify the characteristic components of some of these deposits [e.g., *Adams*, 1974; *Pieters et al.*, 1973, 1974; *Gaddis et al.*, 1985; *Lucey et al.*, 1986; *Hawke et al.*, 1989; *Coombs et al.*, 1990], to begin to constrain the distribution of lunar volcanic deposits [*Head*, 1974], and to understand the styles of eruption and emplacement of basalts on the Moon [*Wilson and Head*, 1981; *Weitz et al.*, 1998].

Previous analyses have established the general distribution, composition, and eruptive styles of lunar pyroclastic deposits, but many fundamental questions remain. The higher-spatial-resolution (~100 m/pixel) views of the Moon presented by the Clementine ultraviolet-visible (UVVIS) data allow scientists to (1) develop a more complete picture of the global distribution of lunar pyroclastic deposits [*Gaddis et al.*, 1998], (2) identify previously unrecognized pyroclastic deposits [*Shoemaker et al.*, 1994; *Morrison and Bussey*, 1997; *Rosanova et al.*, 1998; *Yingst and Head*, 1998], (3) characterize the range of pyroclastic material compositions [*Gaddis et al.*, 1997b; *Weitz et al.*, 1998]; the nature, extent,

[1]Astrogeology Program, U.S. Geological Survey, Flagstaff, Arizona.
[2]PGD/School of Ocean and Earth Science and Technology, University of Hawaii, Honolulu.
[3]Department of Geological Sciences, Northwestern University, Evanston, Illinois.
[4]Department of Geology, College of Charleston, Charleston, South Carolina.

Copyright 2000 by the American Geophysical Union.

Paper number 1999JE001070.
0148-0227/00/1999JE001070$09.00

and timing of their association with mare basalts; and their styles of eruption, and (4) evaluate the implications of these data for interpretation of lunar volcanic and thermal history. In this paper, the third of these topics is addressed, and a compositional analysis of 18 pyroclastic deposits (15 small and three large) using multispectral data from the Clementine UVVIS (415- to 1000-nm wavelengths) camera is presented.

1.1. Characteristics and Distribution of Lunar Pyroclastic Deposits

More than 85 lunar pyroclastic deposits are recognized [e.g., *Gaddis et al.*, 1985; *Hawke et al.*, 1990; *Gaddis et al.*, 1998; Figures 1a and 1b], and numerous additional "dark-mantled" areas have been identified as possible pyroclastic deposits [e.g., *Blewett et al.*, 1995a, b; *Yingst and Head*, 1998]. Lunar pyroclastic deposits are dark and smooth-surfaced, and they are commonly observed in association with sinuous rilles, irregular depressions, or endogenic craters within highlands and/or the floors of old impact craters situated along the margins of many mare-filled impact basins on the lunar near and far sides [e.g., *Head*, 1974]. Previous analyses recognized that many lunar pyroclastic deposits contain dark, glass-rich, friable materials such as those collected at Taurus-Littrow during Apollo 17 [e.g., *Lucchitta*, 1973]. Studies of the orange and black spheres from Apollo 17 samples revealed volatile-enriched coatings, which were inferred to have resulted from fire fountaining during the emplacement of associated mare basalts [e.g., *Heiken et al.*, 1974]. The primitive composition of the pyroclastic glasses indicates that they have undergone little or no fractionation or contamination after leaving their source region, and thus they are inferred to reflect the primary compositional characteristics of the deep (>300-km) interior or mantle of the Moon [e.g., *Delano and Livi*, 1981; *Papike et al.*, 1998]. Compositional analyses of several of the "black spots" from Earth-based spectral reflectance data identified the black spheres as the dominant component [e.g., *Pieters et al.*, 1973, 1974].

Lunar pyroclastic deposits are divided into two classes on the basis of size, morphology, and occurrence [e.g., *Gaddis et al.*, 1985]. The large deposits (~10 in number) are of regional extent (generally >2500 km^2 in size), while small deposits (~90 in number) are more localized (<2500 km^2). Several large pyroclastic deposits (e.g., those at Taurus-Littrow, Sulpicius Gallus, Sinus Aestuum, and Aristarchus) are observed in the highlands on the margins of several mare-filled impact basins and thus were inferred to mark the locations of source vents for associated pyroclastic and mare volcanic activity [*Head*, 1974]. A range of compositions of these large or regional lunar pyroclastic deposits has been inferred from remote-sensing data [e.g., *Gaddis et al.*, 1985; *Lucey et al.*, 1986; *Hawke et al.*, 1991; *Bussey and Spudis*, 1997; *Weitz et al.*, 1998], with iron-rich volcanic beads (both vitreous and crystalline) inferred to be a spectrally dominant component. Eruption and emplacement of regional pyroclastic materials are thought to have been due to strombolian-style, fire-fountain events associated with high-effusion-rate, long-duration eruptions such as those often associated with large vents and sinuous *rilles [Wilson and Head*, 1981; *Weitz et al.*, 1998]. Such eruptions are thought to have occurred primarily during an early period of lunar volcanism (~3.6 b.y. ago) and to have been favored at impact basin margins by relatively thin crust and extensional stresses [e.g., *Head and Wilson*, 1992; *Lucey et al.*, 1994].

The small, localized pyroclastic deposits such as those along fractures in the floor of the crater Alphonsus are widely distributed across the lunar near and far side [e.g., *Gaddis et al.*, 1985; *Hawke et al.*, 1989; *Coombs and Hawke*, 1988; *Coombs et al.*, 1988, 1990; *Gaddis et al.*, 1997b]. Examples of small pyroclastic deposits found on the far side include those in the floor of Schrödinger crater [*Shoemaker et al.*, 1994], at Oppenheimer crater [*Morrison and Bussey*, 1997; *Rosanova et al.*, 1998], and in the Apollo basin within the South Pole/Aitken Basin [*Robinson et al.*, 1996]. These "dark-halo crater" deposits are interpreted to be the result of vulcanian-style or possibly intermittent eruptions, with explosive decompression and removal of a plug of lava or cap rock within a conduit and formation of a vent crater [*Head and Wilson*, 1979]. In addition to their common occurrence as endogenic dark-halo craters along fractures in Imbrian to pre-Imbrian (>3.2 b.y.) impact craters in highland areas along the perimeters of major lunar maria, localized pyroclastic deposits have been identified as isolated, small, dark materials in highland and maria areas, often with no observable source vent [e.g., *Hawke et al.*, 1989]. Although eruptions of localized pyroclastic deposits are thought to have occurred primarily during an early period of lunar volcanism and to have been favored by relatively thin crust associated with impact basins [see *Head and Wilson*, 1992], a possible "young" (~1 b.y.) deposit has been identified near Taruntius crater (5.2°N, 46.5°E [*Spudis*, 1989]).

As with the regional deposits, a wide range of compositional variation exists among localized pyroclastics. However, instead of new or juvenile volcanic glasses being the spectrally dominant compositional component in the small pyroclastic deposits, identifiable differences in the relative amounts of possible juvenile materials versus host rock form at least three classes of localized deposits (Table 1) [*Coombs and Hawke*, 1988; *Coombs et al.*, 1988, 1990; *Hawke et al.*, 1989]. The juvenile materials may consist of disrupted fragments of a preexisting basaltic cap rock or new magmatic materials from depth. The small pyroclastic deposits were subdivided into three compositional classes on the basis of the depth (i.e., strength), position, and shape of their "1.0-micron" or mafic absorption band in Earth-based spectra [e.g., *Hawke et al.*, 1989] (Figure 2). The mafic absorption band in lunar soils is primarily due to Fe^{2+} in iron-bearing components such as the minerals pyroxene and olivine and the volcanic glasses [e.g., see *Pieters and Englert*, 1993, chap. 14].

1.1.1. Small pyroclastic deposits: Group 1. Mafic bands of small pyroclastic deposits in the Group 1 class (Table 1) are centered near 0.94 μm, have relatively shallow depths, and are asymmetrical, with "checkmark"-like shapes (straight, steep short-wavelength edges and shallow, straight long-wavelength edges). Spectra for Group 1 deposits resemble those of typical highlands and are indicative of the presence of feldspar-bearing mafic assemblages dominated by orthopyroxene. Also, the shapes of the mafic bands of Group 1 deposits indicate the presence of an additional iron-bearing component with a band near 1.0 μm (such as volcanic glass, olivine, or clinopyroxene) which has acted to modify the typical orthopyroxene mafic band. Although compositional variation is observed within different Group 1 deposits, most appear to be mixtures of highlands-rich country rock and

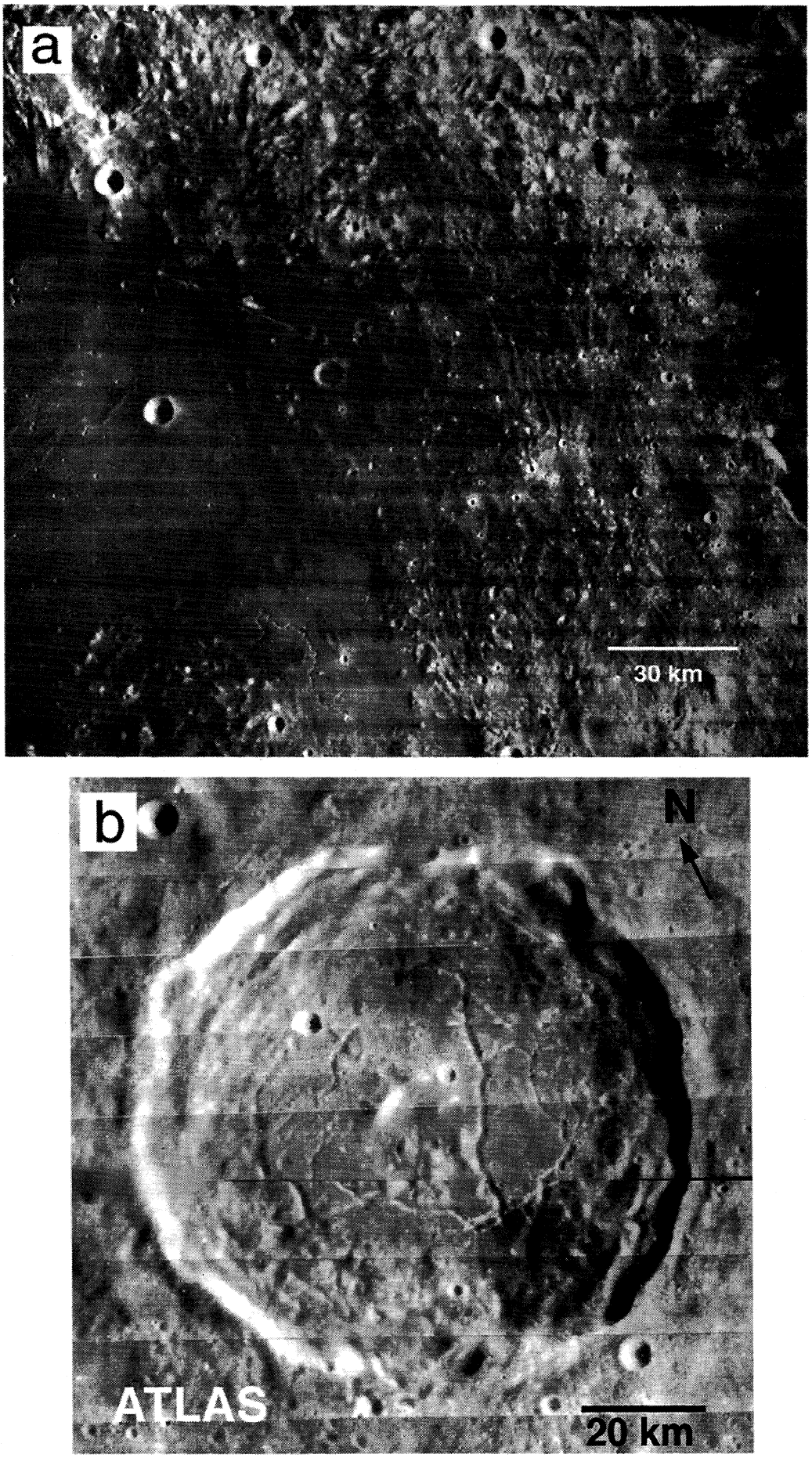

Figure 1. Lunar pyroclastic deposits: (a) the large pyroclastic deposit of the Rima Bode region of the Moon (-3°W, 13°N; LOIV-109 H2) and (b) the small pyroclastic deposits (North and South) in the floor of Atlas crater (diameter 67 km; 44.7°E, 46.0°N; LOIV-79H2 and H3). North is toward the top.

Table 1. Earth-Based Spectral Classification of Small Lunar Pyroclastic Deposits

Group	Sites	Mafic Band			Lithology
		Center, μm	Depth, %	Shape	
1	Atlas South Franklin Alphonsus West	0.94	4-5	asymmetrical	mixed highlands wall rock (opx), glass-rich juvenile material, lesser basaltic cap rock (cpx)
2	East of Frigoris, West East of Frigoris, East	0.96	7	approximately symmetrical	mostly fragmented basalt (cpx), little highlands and glassy material admixed
3	J. Herschel	1.0	5-7	symmetrical	juvenile material rich in olivine, admixed highlands (opx)

After *Hawke et al.* [1989].

glass-rich juvenile material with small amounts of basaltic cap rock material. Examples of Group 1 small pyroclastic deposits are found on the crater floors of Atlas (45°N, 45°E) and Franklin (29°N, 48°E) and near Grimaldi (1°S, 64°W).

1.1.2. Small pyroclastic deposits: Group 2. Mafic bands in spectra for Group 2 deposits are centered near 0.96 μm, have greater depths than those of Group 1, and are symmetrical in shape. Group 2 spectra are similar to those of mature mare deposits, and they are dominated by clinopyroxene. Small pyroclastic deposits in Group 2 appear to consist largely of fragmented plug rock material, with smaller amounts of highlands and/or juvenile materials. Examples of Group 2 deposits are the two small deposits east of Aristoteles crater (50°N, 21°E and 28°E) along the southeast margin of Mare Frigoris.

1.1.3. Small pyroclastic deposits: Group 3. Mafic bands of Group 3 deposits are centered near 1.0 μm, have intermediate depths, are relatively broad and asymmetrical, and are probably multiple bands. Spectra of Group 3 deposits are dominated by orthopyroxene and possibly olivine; the

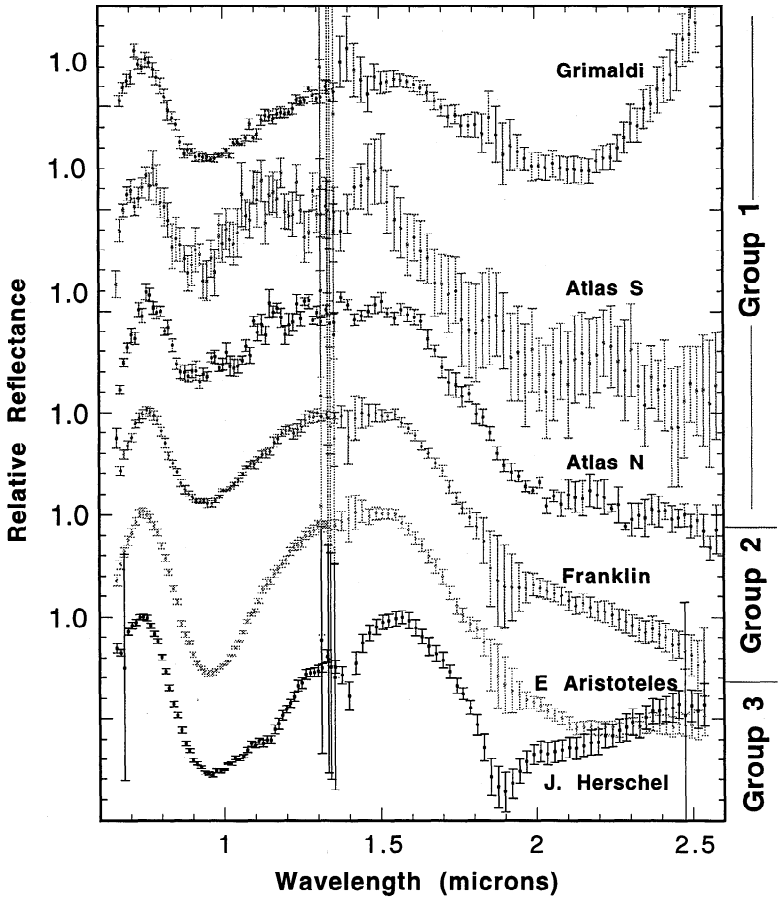

Figure 2. Earth-based spectra for several small lunar pyroclastic deposits [after *Hawke et al.*, 1989]. The spectra have had straight-line continua removed to facilitate comparison of the band depths at ~1.0 μm. Group 1 deposits include those of Atlas (South), Grimaldi, and Franklin, Group 2 deposits include those of East of Aristoteles (Eastern Mare Frigoris East and West), and Group 3 deposits include those of J. Herschel.

orthopyroxene is likely to have been emplaced as a result of erosion and entrainment of the wall rock, and the olivine may be associated with new magmatic or juvenile volcanic material. An example of the Group 3 small pyroclastic deposits is that of J. Herschel crater (62°N, 42°W).

1.2. Objectives

The availability of Clementine high-spatial-resolution, multispectral data for the Moon allows us to characterize the compositions of lunar pyroclastic deposits at a level of detail that was previously unattainable [*Nozette et al.*, 1994; *McEwen and Robinson*, 1997]. A key issue involves the nature and distribution of new magmatic or juvenile pyroclastic materials. Although it is thought that low-albedo glasses and devitrified beads are the dominant components of many regional pyroclastic deposits, other components (such as finely or coarsely fragmented basalt clasts, and reworked country rock of either highlands or mare composition) also may be present in varying proportions [e.g., *Nagle*, 1978]. Identification and characterization of juvenile volcanic components are vital for understanding the primary mafic materials on the Moon and for constraining their eruption conditions and mechanisms.

In this paper, the Clementine UVVIS data are used to perform a compositional analysis of 15 small lunar pyroclastic deposits at 11 sites on the Moon (Figures 3 and 4; Table 2). The small pyroclastic deposits are the focus of this study because of their possible relative youth (~1 b.y. [*Spudis*, 1989]), their broad global distribution and relatively large population, and the fact that their small sizes may have limited the accuracy of early Earth-based (most commonly 1 to 10 km spectral spot size) spectral analyses. This analysis is complementary to that of *Weitz et al.* [1998], who used Clementine UVVIS data to study seven regional pyroclastic deposits. *Weitz et al.* [1998] supported previous identifications of iron-bearing glasses as major juvenile components of these deposits, and they characterized the distributions of glassy and devitrified materials to constrain models of their eruption dynamics in volcanic plumes. By comparing compositional data for both small and large pyroclastic deposits, the nature of juvenile materials in both types of deposits can be constrained. The objectives of this work are to (1) examine the spatial distribution of pyroclastic materials at a single site to determine whether evidence of multiple eruptions can be observed, (2) understand the extent of compositional variations among small lunar pyroclastic deposits, and (3) characterize the juvenile components of the small pyroclastic deposits.

2. Methods

2.1. Clementine Data Processing

The Clementine data were obtained by the UVVIS camera at five wavelengths or bands: 415, 750, 900, 950, and 1000 nm (0.415, 0.75, 0.90, 0.95, and 1.0 μm). The U.S. Geological Survey Integrated Software for Imagers and Spectrometers (ISIS) software [*Eliason*, 1997; *Gaddis et al.*, 1997a; *Torson and Becker*, 1997; *McEwen et al.*, 1998] was used to process the raw Clementine images and to create multispectral mosaics. Input files are predominantly single long-exposure files, with occasional use of merged long- and short-exposure data to improve saturated areas. Radiometric calibration and data processing steps were conducted in 11 phases [*McEwen et al.*, 1998; *Eliason et al.*, 1999], including electronic offset and gain corrections, dark-current subtraction, nonlinearity and temperature-dependent offset corrections, readout or frame transfer correction, flat-field and exposure-time corrections, normalization to a 1-AU distance and conversion to 1-AU relative radiance, conversion to reflectance, photometric normalization (to standard viewing angles of phase=30°, emission=0°, and incidence=30°), subpixel-level coregistration to nearest 0.2 pixel, projection to Sinusoidal Equal-Area, and automated mosaicking. The photometric correction is applied to permit accurate comparison of frame-to-frame reflectance values; the correction is a hybrid function involving separate corrections at different phase angle ranges [*McEwen*, 1991, 1996; *McEwen et al.*, 1998]. The hybrid photometric correction was derived from analyses of Galileo Solid-State Imager (SSI) data (primarily at the 756-nm wavelength) at phase angles of 20° to 100°, supplemented by analyses of low-phase (0° to 4°) Clementine data [*Buratti et al.*, 1996], and disk-integrated photometric models of P. Helfenstein (personal communication, 1998). Clementine data used in this analysis have original phase angles of 14° to 60° (Table 2). The data were spectrally calibrated from digital numbers (in counts/ms) to bidirectional reflectance (percent reflectance, within 5% of absolute) at the standard viewing geometry using reflectance properties of soil at the Apollo 16 landing site to facilitate compositional analyses (C.M. Pieters et al., Clementine UVVIS data calibration and processing, available at http://www.planetary.brown.edu/clementine/calibration.html, 1997) (hereinafter referred to as Pieters et al., online document, 1997).

Possible sources of error in the Clementine data include residual calibration errors (~1% filter-to-filter; Pieters et al., online document, 1997), photometric variations within a scene, uncorrected topographic effects, and scattered light. Residual photometric effects include wavelength-dependent variations (currently unaccounted for in the photometric normalization) at levels of about 0.2% across a Clementine frame and ~0.5% between frames. Topographic effects, particularly those due to steep slopes, can change the effective phase angle and thus alter the apparent brightness of a feature. Although characterization of the effects of topography on analyses of Clementine data are underway [e.g., *Jolliff*, 1999; *Robinson et al.*, 1999], no attempt has been made yet to include a topographic correction in the current Clementine data processing. Scattered light is a possible anomalous brightness in which high-albedo units influence the measured values of low-albedo units (and vice versa) to varying degrees at different wavelengths [e.g., *Gaddis et al.*, 1995; *Li et al.*, 1999]. In the Clementine data, at a wavelength of 415 nm (where scattered light appears to be most significant), scattered light has an estimated magnitude of ~10% in residual brightness near the lunar limb, and it falls to a value of ~3% at a distance of 200 pixels [*Robinson et al.*, 1999].

2.2. Interpretation of Lunar Multispectral Data

In the UVVIS spectral range of the Clementine data, iron-bearing silicate minerals (such as pyroxene and olivine) and volcanic glasses have characteristic Fe^{2+} electronic transition absorption bands near 1.0 μm [e.g., *Burns*, 1993]. The presence and composition of these components can be characterized by the position, shape, and depth of their mafic

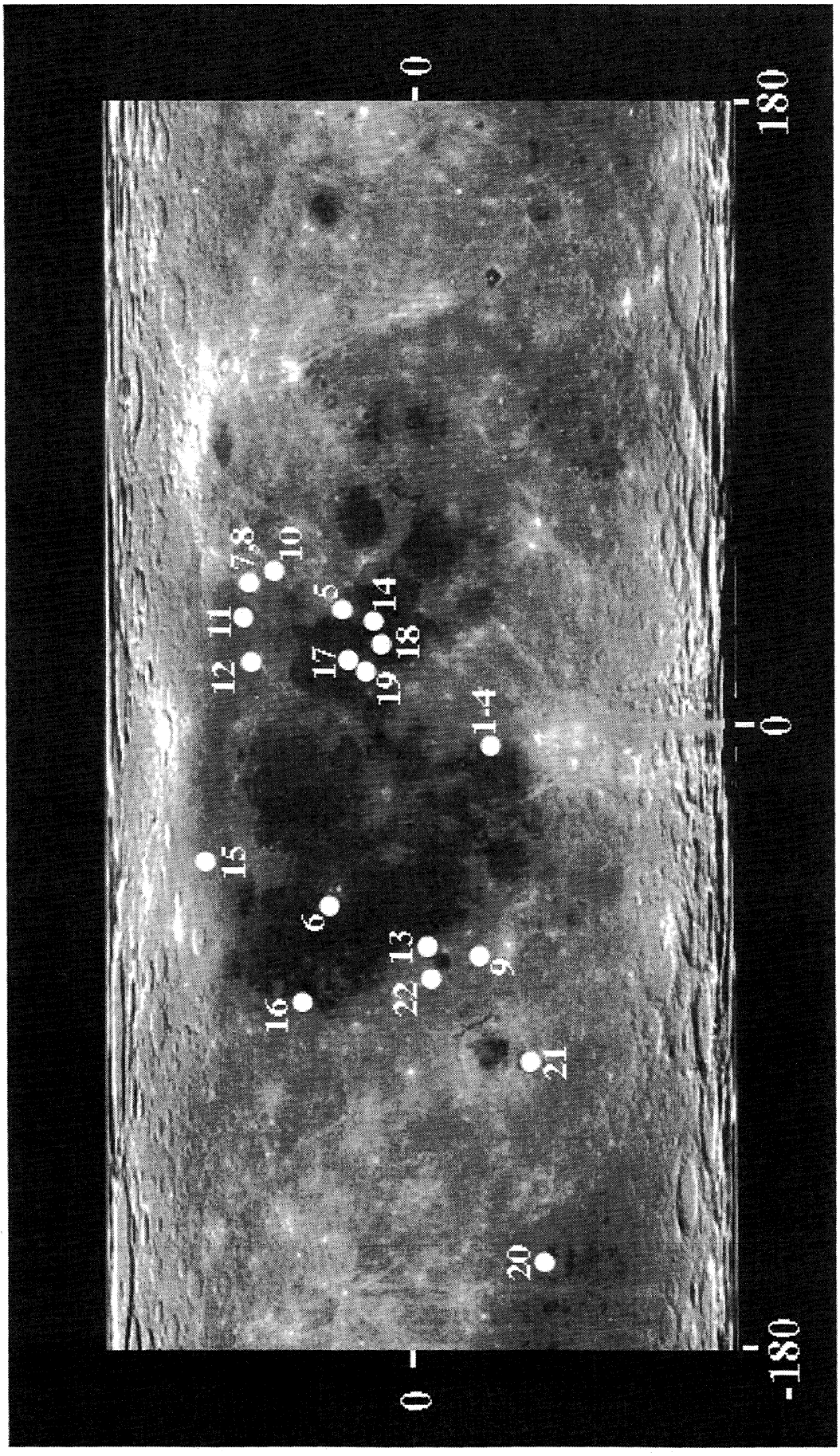

Figure 3. The spatial distribution of the sites included in this analysis. Site numbers correspond to those listed in Table 2. The base image is the global lunar mosaic of Clementine albedo (750 nm) data.

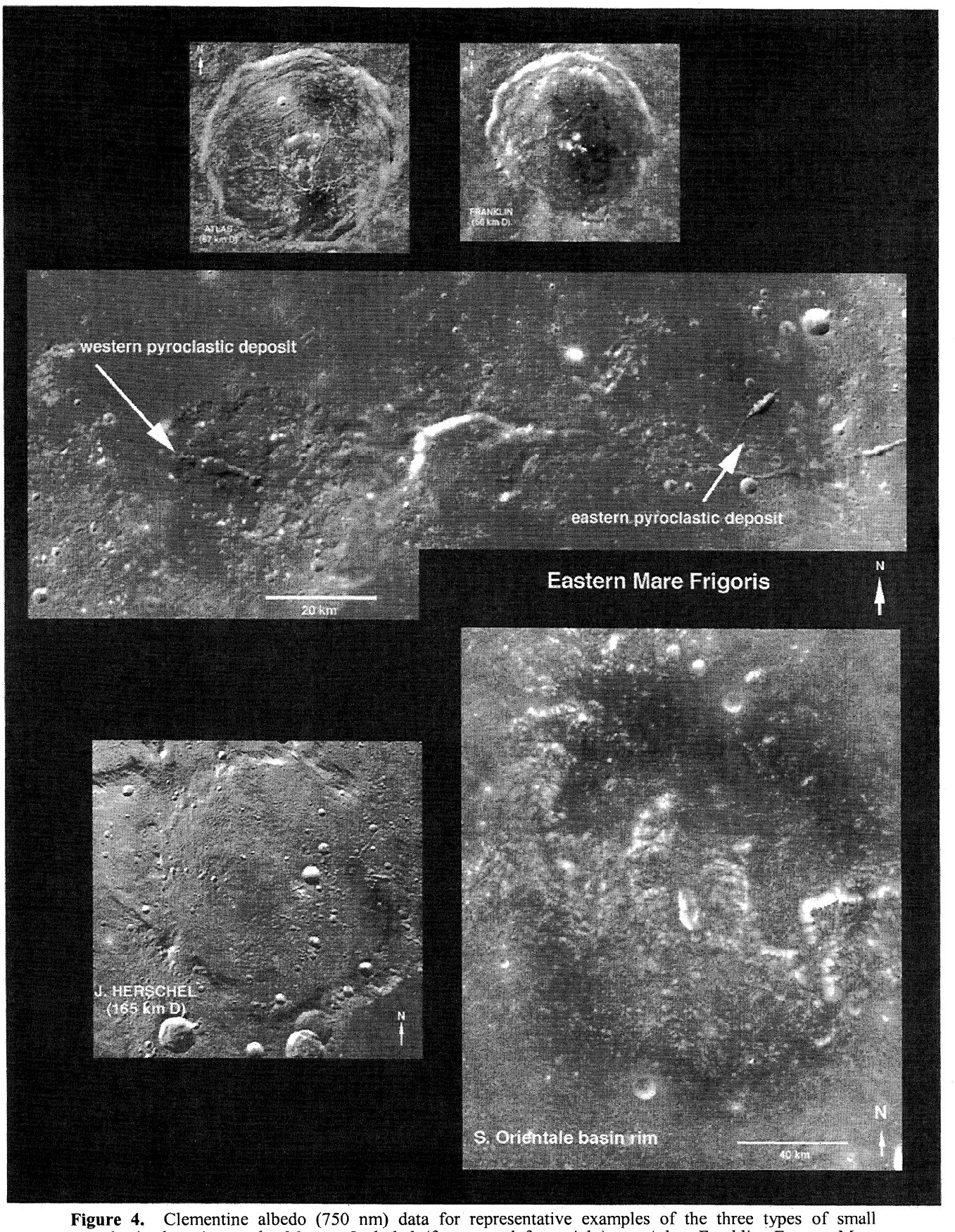

Figure 4. Clementine albedo (750 nm) data for representative examples of the three types of small pyroclastic deposits on the Moon. Included (from top, left to right) are Atlas, Franklin, Eastern Mare Frigoris, and J. Herschel. The annular ring pyroclastic deposit at Orientale is also included for comparison. See Table 2 for site locations.

Table 2. Lunar Sites, Spectral Classification, and Clementine Color Ratio Data Included in This Analysis

Name	Group*	Type†	Location (lat., lon.)	Phase Angle‡	415/750	950/750
1. Alphonsus Northeast 1	2	sp	-12.8°, -1.6°	16	0.57	1.06
2. Alphonsus Northeast 2	1	sp	-12.5°, -1.9°	16	0.59	1.05
3. Alphonsus Southeast	1	sp	-14.4°, -1.9°	15	0.58	1.05
4. Alphonsus West	1	sp	-13.6°, -4.1°	16	0.58	1.09
5. Apollo 17/Taurus Littrow	-	lp	20.4°, 30.1°	20	0.65	1.15
6. Aristarchus	(2)	lp	26.7°, -50.5°	27	0.56	1.07
7. Atlas North	2	sp	47.3°, 44.8°	51	0.56	1.06
8. Atlas South	1	sp	45.7°, 44.6°	50	0.58	1.08
9. Crüger	1	sp	-17.9°, -66.7°	20	0.59	1.09
10. Franklin	1	sp	38.4°, 47.9°	41	0.57	1.10
11. Eastern Frigoris East	2	sp	50.1°, 34.4°	55	0.56	1.06
12. Eastern Frigoris West	2	sp	49.6°, 27.4°	52	0.56	1.06
13. Grimaldi	1	sp	-0.8, -62.3°	19	0.59	1.08
14. Jansen	-	fmc	13.5°, 28.7°	18	0.63	0.95
15. J. Herschel	3	sp	61.4°, -36.9°	60	0.55	1.03
16. Lavoisier	1	sp	38.2, -80.8°	34	0.59	1.08
17. Mare Serenitatis	-	mm	24.5°, 13.5°	35	0.60	1.05
18. Mare Tranquillitatis	-	mm	13.5°, 22.0°	30	0.68	1.06
19. Menelaus	-	fhc	16.3°, 16.0°	16	0.64	1.08
20. Oppenheimer	1	sp	-35.6, -166.0°	36	0.58	1.06
21. Orientale	(1)	lp?	-30.2°, -97.4°	35	0.59	1.09
22. Riccioli	1	sp	-2.9, -74.2°	22	0.58	1.07

*Group: revised spectral classification for small pyroclastic deposits [after *Hawke et al.*, 1989]. Parentheses denote possible Group similarities for a large deposit.

†Type: sp, small pyroclastic deposit; lp, large pyroclastic deposit; fmc, fresh mare crater; mm, mature mare deposit; fhc, fresh highlands crater.

‡Phase angle of the original, uncorrected Clementine data.

absorption bands. Although pyroxenes have absorption bands at both 1 and 2 μm, the precise band centers near 1.0 μm are diagnostic of pyroxene chemistry (e.g., Fe, Mg, Ca substitution), with band centers moving to longer wavelengths as Ca and Fe substitute at increasing levels for Mg in the pyroxene structure [e.g., *Adams*, 1974; *Hazen et al.*, 1978; *Cloutis and Gaffey*, 1991]. In the UVVIS wavelength range, low-Ca pyroxenes (commonly orthopyroxenes) have band centers between 0.9 and 0.94 μm, and high-Ca pyroxenes (clinopyroxenes) have band centers between 0.95 to 1.05 μm [*Adams*, 1974]. Orthopyroxenes are typical of lunar highland units, and clinopyroxenes are observed commonly in the lunar maria. Olivine has a single, broad absorption feature centered near 1.1 μm because of three overlapping Fe^{2+} absorptions; the center wavelength of each band varies with substitution of Fe for Mg in the olivine crystal structure [e.g., *Burns*, 1970, 1993]. Volcanic glasses which are iron-rich, such as the orange glasses from the Apollo 17/Taurus-Littrow region and the green glasses from Apollo 15/Hadley-Apennine region, have broad, Fe^{2+} mafic absorptions at or beyond 1.0 μm and a weaker band at 1.8 μm [e.g., *Adams et al.*, 1974; *Bell et al.*, 1976]. Variations in titanium content among these glasses are distinguishable in remote spectra by an absorption feature near 0.6 μm, and these effects are often superimposed on the longer-wavelength glass absorption bands [e.g., *Pieters and Englert*, 1993, chap. 14].

Although the ~100 m/pixel spatial resolution of the Clementine UVVIS data is higher than that previously available, the five-band data have limited spectral resolution when compared to some Earth-based spectral data (which may have >100 spectral channels between 400 and 1000 nm). These characteristics of the Clementine UVVIS data have prompted the use of relative brightness and other spectral parameters as indicators of color differences and thus compositional variations in the multispectral data. The overall brightness or "albedo" of a unit at 750 nm is a first-order indicator of differences in color due to variations in soil mineralogy, maturity, particle size, and viewing geometry effects. As with mature mare soils, the primary compositional differences among the small lunar pyroclastic deposits that can be characterized with Clementine data include relative titanium content [e.g., *Johnson et al.*, 1991], and relative mafic content and composition [e.g., *Pieters et al.*, 1993; *Pieters and Englert*, 1993, chap. 14]. The relative titanium content of a basaltic soil is described by the slope of the line between 415 and 750 nm, defined as the ratio of UV/VIS or the 415/750 nm ratio. Deposits with high 415/750 values have higher titanium contents and have historically been called "blue"; deposits with low values have lower titanium contents and are "red" [e.g, *Wilhelms*, 1987]. The mafic content is defined by the 1-μm band strength, or the ratio of 950/750 nm. Deposits with low 950/750 values have deep 1.0-μm bands and strong mafic spectral signatures, and those with high 950/750 values have shallow bands and weak mafic signatures. In addition to providing effective compositional discrimination among the small pyroclastic deposits, the spectral ratio parameters (as measures of relative reflectance) serve to minimize small residual photometric variations due to viewing geometry effects. As noted further below, these relative compositional classifications for pyroclastic deposits are complicated by the possible presence of volcanic glasses in the deposits.

The use of Clementine spectral ratios for compositional analyses is warranted by the lack of spectral resolution and information beyond 1 μm in the UVVIS data. It is impractical to remove a slope or continuum curve from the UVVIS data as is commonly done to Earth-based spectral data to enhance the apparent shape and position of the 1.0-μm band [e.g., *McCord et al.*, 1981; *Fischer and Pieters*, 1994, 1996; *Tompkins and Pieters*, 1999]. The slope of such a continuum, along with overall reflectance and mafic absorption band strength, bears evidence of the amount of "space weathering" a mature mafic soil has undergone With increasing age, the continuum slope increases, and the overall reflectance and mafic band depth decreases. Although knowledge of these slope values is not available from the Clementine UVVIS data, the UV/VIS and 950/750 ratio values can also be interpreted in terms of relative soil maturity: a mature soil is "red" and has a relatively shallow 1.0-μm band, while a more immature soil is "blue," with a deeper 1.0-μm band [e.g., *Fischer and Pieters*, 1994]. These effects are complexly convolved with those due to the presence of titanium- and iron-bearing minerals in lunar soils [e.g., *Lucey et al.*, 1998a, b].

Recent work with the global Clementine UVVIS data has led to the development of geochemical estimates of FeO and TiO_2 abundances, along with relative soil maturity, based on empirical relationships between spectral properties and elemental abundances for lunar soils [e.g., *Lucey et al.*, 1994; 1998 a, b]. These estimates are based on correlations between geochemical data from lunar samples and reflectance at 0.415, 0.75, and 0.95 μm and they represent attempts to deconvolve the sometimes competing effects of composition and maturity on reflectance. The models account for the effects of the presence of ferrous iron, titanium, and opaques in minerals, as well as submicroscopic metallic iron produced by space weathering. A key assumption in the development of the models used to derive these estimates is that glass abundance in lunar soils is highly correlated with maturity. Impact glasses are the dominant form of glass on the Moon, and they are a major component of agglutinates formed as soils increase in age. Because the effects of volcanic glasses on this relationship are presently unknown, both the FeO and TiO_2 abundances and the maturity of soils developed on lunar pyroclastic deposits cannot yet be completely constrained by the same means.

Although both intimate and coarse mixing of components of variable composition play significant roles in the development of all lunar soils [e.g, *Pieters and Englert*, 1993, chap. 14] and the deconvolution of soil components as identified remotely has been the subject of intensive investigation in recent years [e.g., *Sunshine and Pieters*, 1993; *Mustard et al.*, 1998], the approach used here is to evaluate small pyroclastic deposit compositions on the basis of the dominant type of mafic minerals as observed in the spectral ratio parameters identified above. This first-order classification will serve as a comparison to previous Earth-based spectral analyses and will provide a basis for further characterizations of lunar volcanic deposits with the Clementine data.

3. Compositional Analyses of Small Pyroclastic Deposits

To characterize the compositions of the small pyroclastic deposits on the basis of Clementine UVVIS data, we focus on 15 small pyroclastic deposits at 11 sites broadly distributed across the Moon (Table 2; Figures 3 and 4): Alphonsus crater floor, Atlas crater North and South floor; near Crüger crater, Franklin crater floor; two deposits on the southeastern margin of Mare Frigoris, or Eastern Frigoris West and East, near Grimaldi crater, the southeast of the floor of J. Herschel crater, Lavoisier crater floor, Oppenheimer crater floor, and near Riccioli crater. In each case, probable vents, generally in the form of endogenic "dark-halo" craters or dark-rimmed irregular depressions, are identifiable [e.g., *Head and Wilson*, 1979]. Spectral data for three large pyroclastic deposits and several typical mare and highlands sites are included for comparison: (1) the annular ring of pyroclastic material along the southern margin of Orientale basin [e.g., *Bussey and Spudis*, 1997; *Weitz et al.*, 1998], the regional deposits at (2) Apollo 17/Taurus-Littrow and (3) Aristarchus, (4) the young highlands crater Menelaus, (5) the young mare crater Jansen, (6) the high-titanium mare of northern Mare Tranquillitatis, and (7) the low-titanium mare of southeastern Mare Imbrium. The Orientale pyroclastic deposit is enigmatic: because it is large, it has been modeled as a regional deposit [e.g., *Head et al.*, 1997; *Weitz et al.*, 1998], but its nearly circular form and its clearly visible vent are similar to those of small pyroclastic deposits. This comparison of compositional data for large and small pyroclastic deposits, including the Orientale deposit, may help to clarify the nature of this deposit. Spectra were obtained with sampling areas of 15x15-pixel or 25x25-pixel box sizes (at 100 m/pixel) within spectrally homogeneous, topographically flat units near the vent(s). The one exception to this spectral extraction method is the Orientale annular deposit ~80 km from the apparent vent; in this area, spectra were extracted within uniformly dark units spaced widely around the ringed deposit. In all cases, it is assumed that the spectra represent mature volcanic soils in which particle size has been homogenized by maturation processes. In each case, spectral extraction was restricted to a single-orbit strip to limit problems with interorbit brightness variations due to changes in viewing geometry [e.g., *Jolliff*, 1999]. Standard deviations of <2% at each wavelength are typical.

To characterize further the juvenile components in lunar pyroclastic deposits, the Clementine color ratio data can be used to evaluate subtle differences in composition among the small pyroclastic deposits and to compare them to other lunar units. In this section, a summary of the interpretation of the reflectance spectra for the small pyroclastic and comparative deposits is presented. These data are then used (1) to examine the spatial distribution of pyroclastic materials in the floor of Atlas crater to search for evidence of multiple eruptions at a single site and (2) to characterize the extent of compositional variations among representative examples of small and lunar pyroclastic deposits. These analyses set the stage for a summary discussion of the nature of the juvenile components of lunar pyroclastic deposits.

3.1. Spectral Interpretation

Clementine five-band UVVIS reflectance spectra for 14 lunar sites, including 10 pyroclastic deposits at 8 sites, are shown in Figure 5 (see also Figure 3 and Table 2). The small pyroclastic deposits, chosen as representative examples of the three compositional classes of *Hawke et al.* [1989], include those at Alphonsus West (near Alphonsus CA), Atlas South and North, Franklin, Eastern Frigoris East and West, and J.

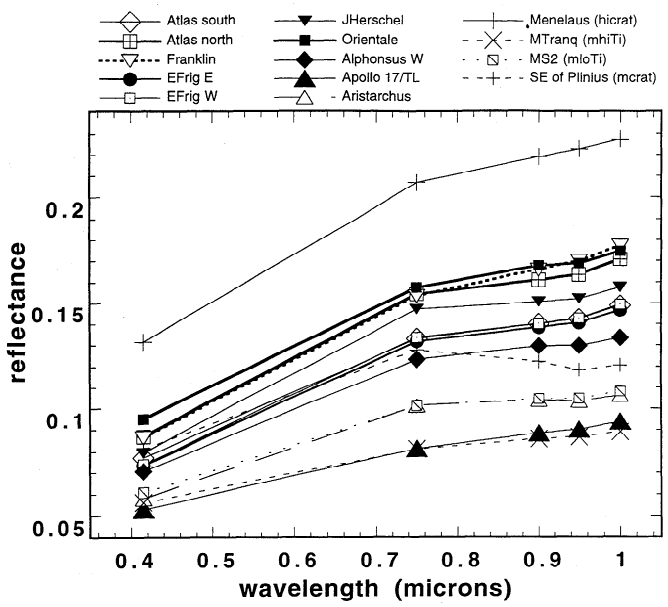

Figure 5. Clementine spectral reflectance data for examples of three types of small pyroclastic deposits on the Moon, along with spectra for the larger pyroclastic deposits at Apollo 17/Taurus Littrow and Aristarchus Plateau and for typical mare and highlands soils. Included are spectra for Atlas South and North floor, Franklin floor, deposits in the West and East of Eastern Mare Frigoris, J. Herschel, Orientale Basin south rim, and Alphonsus. See Table 2 for site locations.

Herschel. Large deposits include those at Orientale, Apollo 17/Taurus-Littrow, and Aristarchus. Also for reference, spectra for a highlands crater (the Copernican crater Menelaus, 26-km diameter), a mare crater (Jansen, 23-km diameter), and the mature mare deposits of Serenitatis (low titanium) and Tranquillitatis (high titanium) are shown. For information on primary mineralogic variations among the small pyroclastic deposits, three aspects of these spectra are emphasized: the albedo of the deposits at 750 nm, the 415/750 nm (UV/VIS) ratio, and the 1-μm band depth.

3.1.1. Albedo. Spectra in Figure 5 show straightforward albedo trends. The Copernican crater Menelaus, in the Montes Haemus on the southern rim of Mare Serenitatis, is the brightest feature, as expected for a relatively fresh highlands crater exposing anorthositic material. The high-titanium mare in northern Mare Tranquillitatis and the pyroclastic deposit at Apollo 17/Taurus-Littrow are the darkest of the units observed, and these are followed closely by the slightly brighter Aristarchus Plateau pyroclastic deposit and the low-titanium mare deposit of central Mare Serenitatis. Jansen, the relatively fresh mare crater southeast of Plinius, has an intermediate brightness level overall, and it is brighter than the two mature mare deposits at Mare Serenitatis and Mare Tranquillitatis. The majority of the pyroclastic deposits observed have intermediate albedoes at 750 nm, with brightness increasing from Alphonsus West, Eastern Frigoris East and West, Atlas South, J. Herschel, Atlas North, Franklin, to Orientale. These brightness variations are interpreted to result largely from compositional differences due to iron and titanium (or opaque mineral) contents of basalts and volcanic glasses in the mare and pyroclastic deposits, with possible superimposed maturity effects [largely the amounts of submicroscopic metallic iron and agglutinates; *Pieters and Englert,* 1993; *Lucey et al.,* 1998a].

3.1.2. UV/VIS. In Figure 5, the UV/VIS ratio for each deposit (Table 2) is examined as the slope of the line between 415 and 750 nm. These spectra show that the steep 415/750 slopes of the immature highlands and mare units such as those at Menelaus crater (415/750 or UV/VIS=0.64) and Jansen (0.63) are readily distinguished from the relatively shallow slopes (lower UV/VIS values) of the more mature mare and localized pyroclastic deposit soils. In the case of the highlands crater Menelaus, these data are indicative of a relatively young or fresh surface with an anorthositic lithology [e.g., *Pieters*, 1986]. For Jansen, these relatively high UV/VIS values are typical of a fresh mare crater in a low-titanium basalt soil. Differences among the pyroclastic deposits as reflected in the UV/VIS values may be attributable to mineralogic and/or maturity differences, although the maturity relationships (in the form of competition between juvenile glasses and agglutinitic glasses due to space weathering) for these deposits are poorly understood at present. *Weitz et al.* [1998] have related the 415/750 values for large pyroclastic deposits to color differences due to pyroclastic glass crystallinity and/or the Fe*Ti content of the glasses, as well as relative maturity. The 415/750 values observed among the small pyroclastic deposits are generally lower (redder) than those of the large pyroclastic deposits, ranging from ~0.55 (J. Herschel) to 0.59 (Orientale) as compared to 0.65 for Apollo 17/Taurus-Littrow. These values are typical of mature lunar mare and highlands deposits and thus support the previously identified spectral affinities with typical mare (Group 2) and highlands soils (Group 1) for the majority of small pyroclastic deposits [e.g., *Hawke et al.,* 1989].

3.1.3. One-micrometer band depth. Spectra in Figure 5 also allow us to compare mafic mineralogies by estimating the slope of the line between 950 and 750 nm as a measure of depth of the 1-μm absorption band (see also Table 2). The 1-μm band of the fresh highlands crater Menelaus is very shallow or weak (950/750=1.08), as is consistent with a noritic anorthosite lithology and with a small amount of low-Ca pyroxene as the primary mafic mineral. By contrast, the mafic band of Jansen, the fresh mare crater southeast of Plinius, is the strongest observed among these examples (0.95), suggestive of a significant component of high-Ca pyroxene, with a prominent mafic absorption band near 0.98 to 1.00 μm. The mare deposit in Mare Tranquillitatis and the pyroclastic deposit at Apollo 17/Taurus-Littrow have the shallowest or weakest mafic bands, as might be expected for such mature, high-titanium volcanic deposits (with crystalline and glassy beads in the case of the Apollo 17 soil). The mature mare deposit of Mare Serenitatis (~MS2) shows the slightly stronger mafic absorption typical of a low-titanium basalt and is similar to the large Aristarchus Plateau pyroclastic deposit. As observed previously [e.g., *Gaddis et al,* 1985; *Hawke et al.,* 1989], the lunar pyroclastic deposits have highly variable mafic absorptions, but all are generally weaker than most mature mare soils. Mafic band strengths for the small pyroclastic deposits increase in the following order (950/750 from 1.1 to 1.03): Franklin, Orientale, Alphonsus, Atlas South, Eastern Frigoris West and East, Atlas North, and J. Herschel. Although maturity effects cannot be

ruled out, these values are interpreted to be indicative of primary compositional variations among the small pyroclastic deposits and are consistent with changes in the amounts of juvenile components (such as low-Ca and high-Ca pyroxene and/or olivine and volcanic glasses) and/or degrees of mixing with local highlands and mare lithologies as noted by previous authors [e.g., *Hawke et al.*, 1989].

3.2. Intradeposit Compositional Variation: The Atlas Crater Example

A key question in the compositional analysis of small lunar pyroclastic deposits is the nature and extent of possible variations within a single pyroclastic deposit [e.g., *Robinson et al.*, 1996]. Such variations, if present, may be the result of several competing effects, including maturity differences, mixing with adjacent or underlying materials (perhaps due to a thin mantling deposit overlaying a unit of different composition), and intrinsic mineralogic differences. The latter possibility is the most intriguing and may include differences in crystallinity due to eruption style or duration [e.g., *Weitz et al.*, 1998] or variations in mineralogy due to multiple eruptions occurring from a single vent or to changes in composition of a single eruption with time. Here we examine the Atlas crater floor deposits in detail to determine the nature of possible intradeposit compositional variations in this area. We selected this example because we can readily identify two distinct vents (North and South), the deposits are spatially separable (~80 km distant), topographic variations do not appear to be substantial, and the areas are covered by a single Clementine orbit with ~100 m/pixel spatial resolution.

Atlas is an Upper Imbrian crater (3.25 to 3.72 b.y. ago [*Wilhelms*, 1987]) in the highlands northeast of Mare Serenitatis, and its composition is primarily that of mature highlands materials with superimposed low-albedo, mafic deposits surrounding two irregular depressions along floor fractures in the North and South regions of the crater floor [e.g., *Hawke et al.*, 1989] (Figure 6a). To examine the possible compositional variations within the dark deposit, we measured 200-pixel (~20-km) transects in the Clementine 950/750 nm ratio data across the probable vents for the North and South floor deposits in Atlas crater (Figure 6b). Transects extend to distances of 30 to 40 pixels beyond the farthest reaches of the ~120-pixel-long deposits (Figures 6b, 7). The profiles clearly show both the spatial distribution of the deposit in a single dimension and the superimposed effects of topography (i.e., increased bright/dark patterns due to hummock slopes, floor fractures, and vents facing toward or away from the Sun and/or sensor, marked with "t" in Figure 7). Although substantial spatial variation at the pixel-

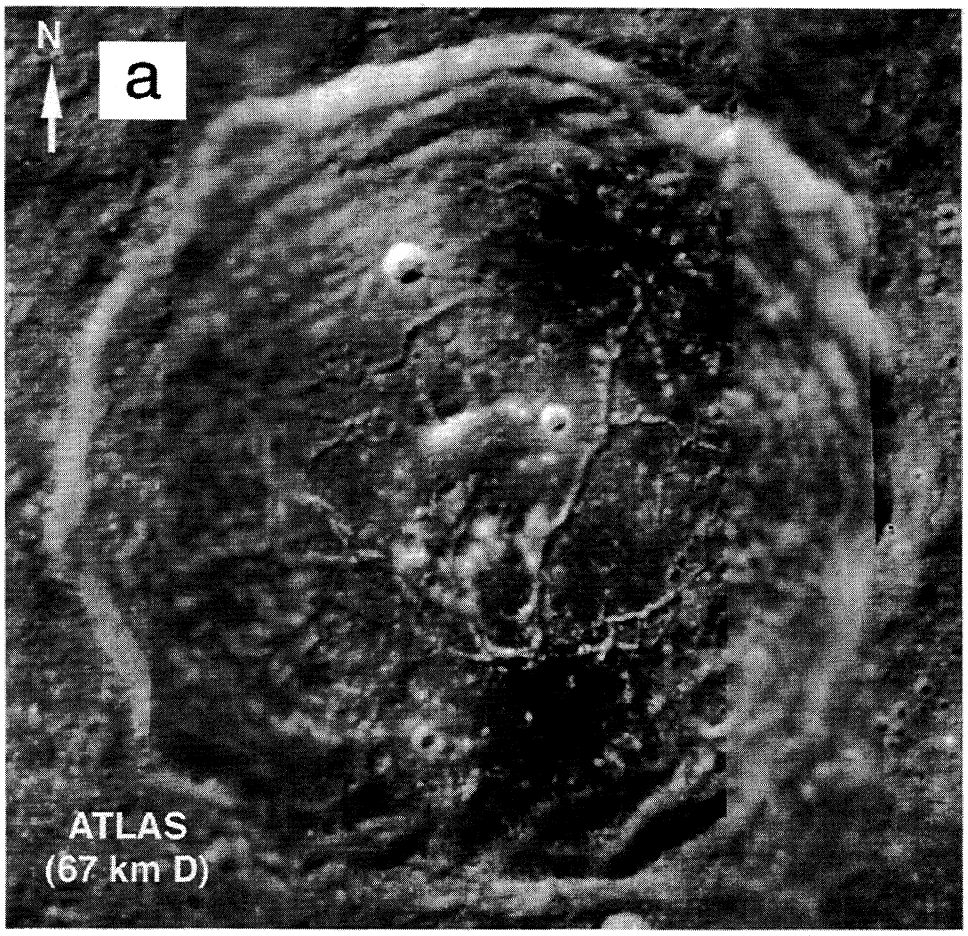

Figure 6. Atlas crater (67 km diameter): (a) Clementine albedo (750-nm) data. Note the dark pyroclastic deposits in the North and South crater floor. (b) Clementine 950/750 ratio image depicting the mafic absorption band in this area. Ratio values of ≤0.9 are black and have stronger mafic absorptions; white areas have ratio values of ≥1.11, and they have weaker mafic bands. Profile locations for Figure 7 are marked.

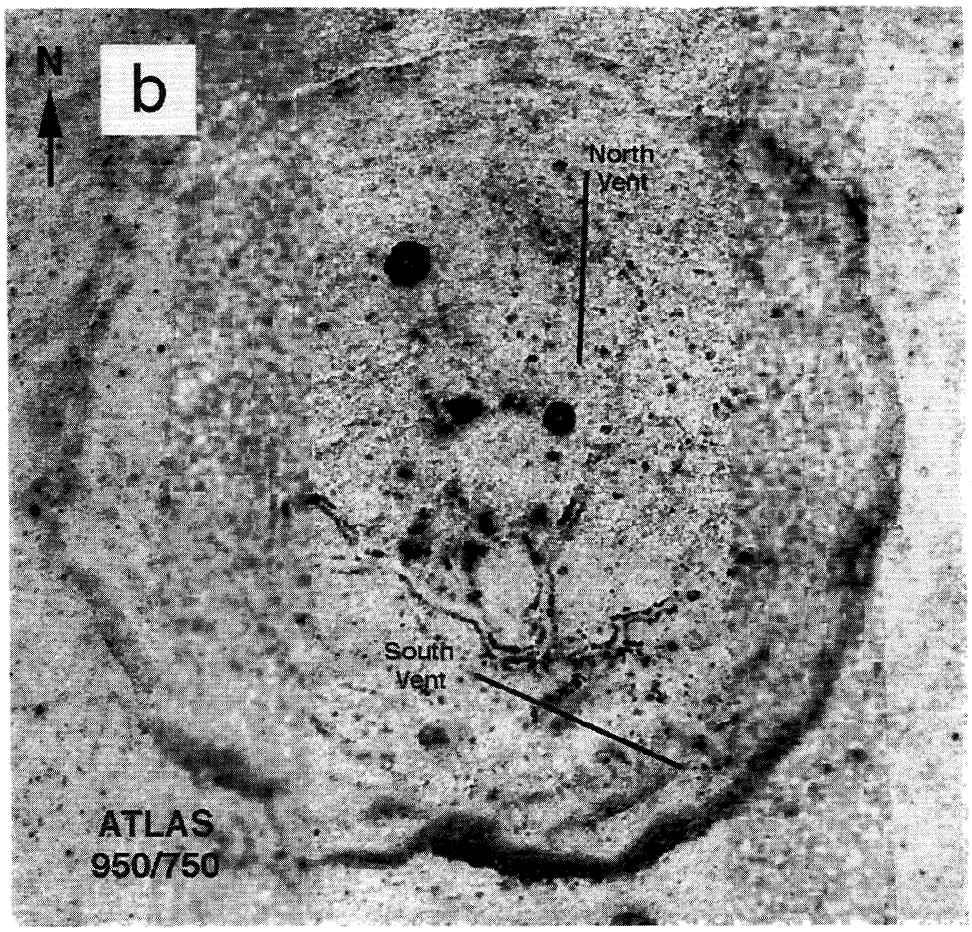

Figure 6. (continued)

to-pixel scale is apparent at a 3% level even where topography is not a major factor, the mean values of the 950/750 ratios show revealing trends. In the case of the North vent deposit, the effect of the superimposed pyroclastic deposit is to lower the 950/750 value to an average of 1.065, well below that of the local mature highlands value of 1.08 (note that 950/750 values for the crater floor vary from 1.075 to 1.093). Note also that the mafic band weakens toward the margins of the deposit, but it does not show abrupt changes that could be interpreted as primary compositional variations within the original deposit. These trends suggest that the North vent pyroclastic deposit has a stronger mafic band than the crater floor and that it is strongest near the vent and weakens as the deposit thins at its margins. By contrast, for the South vent deposit, we see that the average value of the 950/750 ratio (~1.09) is slightly higher than that of the surrounding crater floor (~1.08), and to the southeast, the average 950/750 value (~1.095) is even higher. The pyroclastic deposit in this area appears to have a mafic spectral signature which is much like that of the highlands (as do the Group 1 deposits of *Hawke et al.* [1989]); in this case, the pyroclastic deposit has a weaker mafic band than that of the surrounding highlands. The highest, or weakest, mafic band depth values southeast of the South vent pyroclastic unit may correspond to a thicker deposit; possible changes in mafic band depth with increasing distance from the vent are masked by the topographic features near the margins of the South vent deposit.

To summarize these observations: (1) the mean 950/750 values for the pyroclastic deposits are different than those of subjacent highlands terrain; (2) the mean 950/750 values for each pyroclastic deposit are different from each other; and (3) for the North vent deposit, a compositional trend of decreasing mafic band strength with increasing distance from the vent is observed. The North vent pyroclastic deposit has a relatively strong mafic absorption band as compared to the surrounding highlands in the crater floor, and the South vent deposit has a weaker band than that of the crater floor materials. In the case of the Atlas crater pyroclastic deposits, these data suggest that there are two compositionally distinct pyroclastic deposits within a single vent area. Compositional trends at the North vent can best be explained as a result of thinning of the pyroclastic deposit with increasing distance from the vent; no strong indications of intradeposit compositional variations are observed in this example. Although both pyroclastic deposits occur in the floor of the Upper Imbrian Atlas crater and are thus younger than ~3.25 b.y. [*Wilhelms*, 1987], little detailed information exists on the relative ages of these deposits. The simplest explanation for the origin of the observed compositional variation between the North and South deposits is that magmatic intrusion under the floor of Atlas caused two explosive eruptions, and different proportions of wall rock, cap rock, or juvenile materials were emplaced in each area, perhaps as a result of differences in eruption duration. Nevertheless, we cannot rule out the possibility that two temporally distinct eruptions have

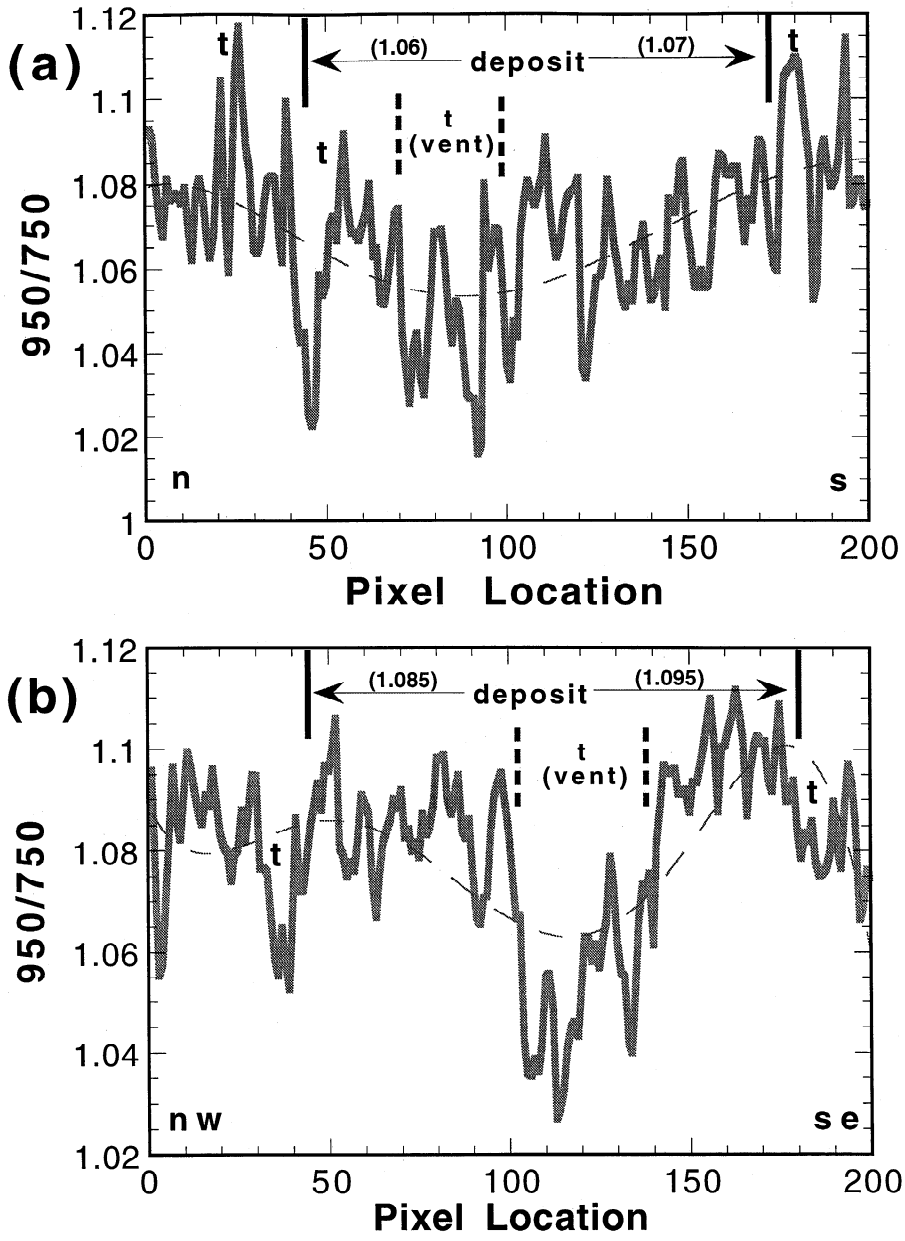

Figure 7. Atlas crater: Profiles of 950/750 ratio values across the (a) North and (b) South vents. The locations of topographic features are marked ("t"), and the extents of the deposits and the vents are indicated. Mean ratio values for each portion of the deposit are also shown. The dashed curves, provided for reference, are fifth-order polynomial curves fit to the profiles using the least squares method.

occurred from a single, possibly related vent structure, and that we may be observing changes with composition through time at Atlas crater.

It should be noted that this analysis does not explicitly account for the possible effects of scattered light. If present, scattered light would act to artificially brighten the pyroclastic deposits in a wavelength-dependent manner [e.g., *Gaddis et al.,* 1995; *Robinson et al.,* 1999]. Shadow measurements of craters in the region suggest a possible brightening effect at the 2% level which may be due to scattered light. However, because the two deposits in Atlas crater floor are in relatively close proximity to each other, and they are likely to be uniformly affected by scattered light from surrounding highlands units, scattered light is not thought to be responsible for the observed variations in 950/750 values. In any case, scattered light could not account for the magnitudes of the differences in brightness between the deposits [e.g., *Li et al.,* 1999].

3.3. Interdeposit Compositional Variation

To examine the compositional relations among representative members of the three classes of small lunar pyroclastic deposits, we compared mean values of reflectance ratios (415/750 and 950/750) for 15 deposits at 11 sites: Alphonsus, Atlas, Crüger, Franklin, Eastern Mare Frigoris, Grimaldi, J. Herschel, Lavoisier, Oppenheimer, Riccioli, and the unclassified annular pyroclastic deposit on the southern

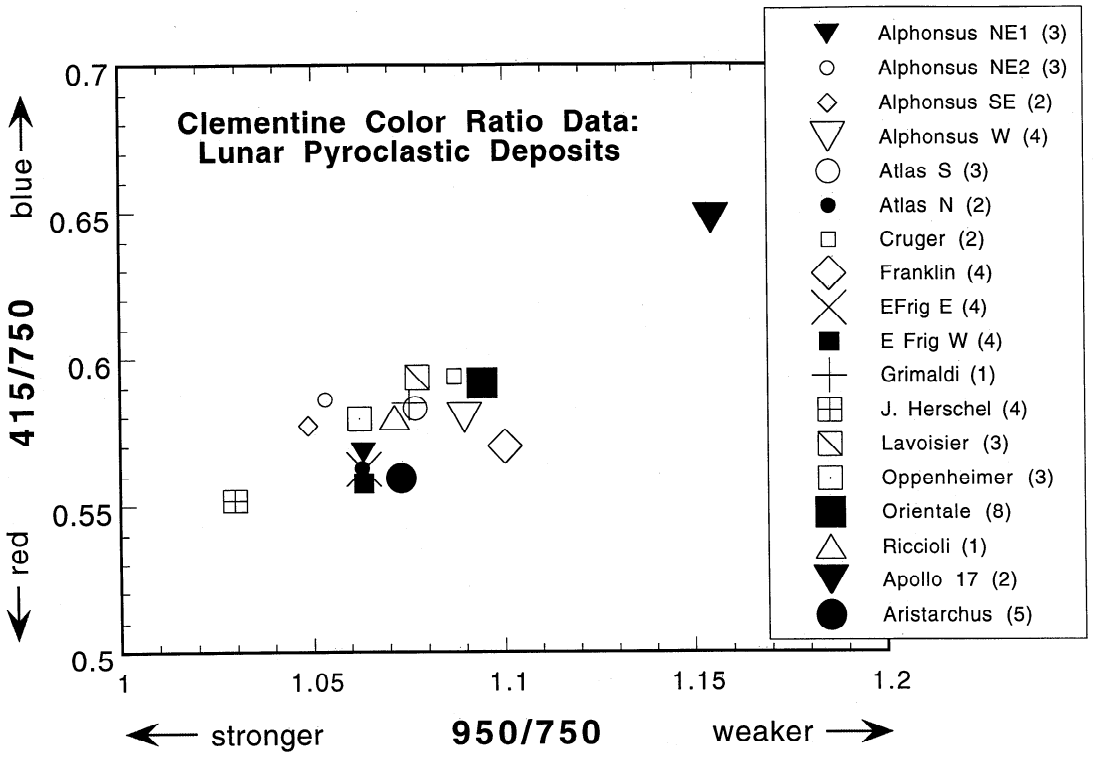

Figure 8. Mean color ratio data (415/750 versus 950/750) for several lunar pyroclastic deposits. Included are data for deposits at Alphonsus, Atlas, Crüger, Franklin, Eastern Mare Frigoris, Grimaldi, J. Herschel, Lavoisier, Oppenheimer, Orientale, Riccioli, Apollo 17/Taurus Littrow, and Aristarchus. The number of sites included in each calculation of mean value is indicated in parentheses near each site label. See Table 2 for site locations.

rim of Orientale basin (Figure 8). For comparison, color ratio data for the large pyroclastic deposits at Taurus-Littrow and Aristarchus Plateau are also shown. All of the pyroclastic deposits shown in Figure 8 have relatively shallow mafic band depths (all 950/750 > 1), and they have 415/750 or UV/VIS ratios in the 0.55 to 0.6 range, comparable to many low-titanium mare basalt and lunar highlands deposits. The large pyroclastic deposit at Apollo 17, among the bluest of lunar volcanic deposits (i.e., high TiO_2) and having one of the weakest mafic absorption bands [e.g., *Gaddis et al.*, 1985], plots far above and to the right of all of the small deposits examined here. Although possible overlap is observed, each of the three compositional groups of *Hawke et al.* [1989] can be distinguished in Figure 8. However, note that our results are slightly different and thus represent small modifications to the previous three-group classification scheme.

3.3.1. Small pyroclastic deposits: Group 1 (revised). The larger cluster (Figure 8, top) has a wider range of mafic band depths, the UV/VIS values are higher (bluer), and the average mafic band depths are shallower than those of the small cluster in the center and the J. Herschel point at lower left. The larger cluster includes 10 small pyroclastic deposits, including those of Alphonsus Northeast 2 (near Alphonsus KC), Southeast, and West, Atlas South, Crüger, Franklin, Grimaldi, Lavoisier, Oppenheimer, and Riccioli. Members of the larger cluster in Figure 8 can be considered to be representative of the Group 1 deposits of *Hawke et al.* [1989]. Note also that the Orientale annular pyroclastic deposit falls with the Group 1 color ratio range.

3.3.2. Small pyroclastic deposits: Group 2 (revised). The central cluster in Figure 8 includes four small pyroclastic deposits: Atlas North, Alphonsus Northeast 1 (near Alphonsus MD), and Eastern Mare Frigoris East and West. Members of the central cluster are comparable to the Group 2 deposits of *Hawke et al.* [1989]. Although small pyroclastic deposits in the central cluster overlap slightly in 415/750 with the Group 1 cluster, they generally have lower 415/750 values and are thus redder in color, with possibly lower titanium contents, than most Group 1 deposits. Also, the central cluster has an average 950/750 ratio value that is lower than most Group 1 deposits, and so it has slightly stronger mafic absorptions than many of the Group 1 deposits. Note that two of the crater floor sites, Alphonsus and Atlas, have small pyroclastic deposits that can be considered to fall into two separate compositional groups. Also, the large pyroclastic deposit of Aristarchus Plateau shows a similarity in color ratio to the small deposits of Group 2.

3.3.3. Small pyroclastic deposits: Group 3 (revised). The single deposit at the lower left (Figure 8) is the J.Herschel deposit; in this analysis, it is the only member of Group 3. The ratio value for the J. Herschel crater deposit is the lowest 950/750 observed, and thus it has the strongest mafic absorption feature among the small pyroclastic deposits. The J. Herschel deposit also has the lowest 415/750 value and is the reddest of the deposits examined.

Although a general trend of increasing mafic absorption band strength from Group 1 to Group 2 to Group 3 small pyroclastic deposits can be observed in Figure 8, the difficulty

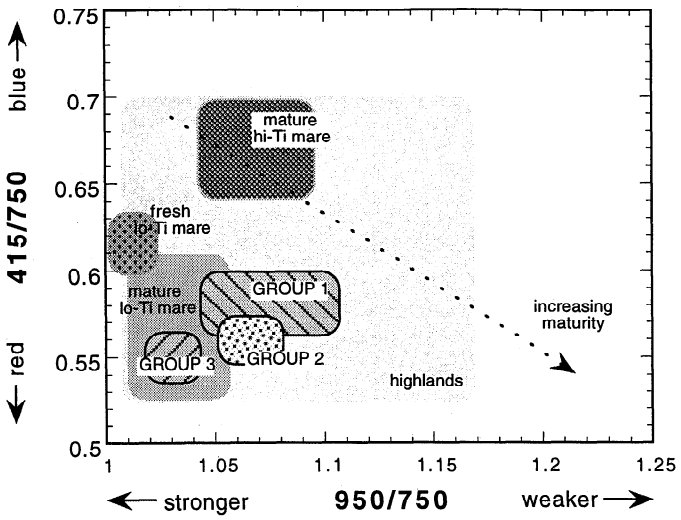

Figure 9. Ranges of typical Clementine color ratios (415/750 versus 950/750) for three classes of small lunar pyroclastic deposits and for typical mature and fresh mare and highlands soils. As indicated by the dashed arrow, lunar soil maturity for mare soils increases downward to the right.

in clearly distinguishing the three compositional classes among these deposits indicates that this classification will break down with additional data. This observation suggests that the compositional variation among the majority of small pyroclastic deposits can best be explained as mixing of juvenile volcanic components with a continuum of nearby mare and highlands components. To explore possible compositional relations of the small pyroclastic deposits with those of typical highlands and mare materials, we examine color ratio data (Figure 9) for typical highlands and mature and fresh maria (both low- and high-titanium; fresh high-titanium deposits are off-scale at the high 415/750 and low 950/750 values). Although the systematics have not been resolved for application to lunar pyroclastic deposits [e.g., *Lucey et al.*, 1998a, b], color ratio data can be interpreted in terms of relative maturity for mare soils: a mature soil is red and has a relatively shallow 1.0-μm band, and an immature soil is blue, with a deeper 1.0-μm band [e.g., *Fischer and Pieters*, 1996]. This trend of increasing maturity with increasing 950/750 and decreasing 415/750 values for the shaded areas of typical mare soils is marked with a dashed arrow in Figure 9. Note that the color ratio data for the small pyroclastic deposits, shown as shaded areas, are approximately orthogonal to the maturity trend, and so maturity variations are unlikely to account for most of the compositional variations observed among these deposits.

As indicated by the degree of overlap in the shaded regions in Figure 9, the small pyroclastic deposits all show the greatest similarities in color ratios with mature highlands and mature low-titanium maria. The Group 1 deposits show a substantial degree of overlap, and thus strong compositional affinities, with typical lunar highlands, as indicated previously by *Hawke et al.* [1989]. As further noted by *Hawke et al.* [1989], Group 2 deposits have spectral characteristics similar to mature mare soils, especially those with low titanium contents. Color ratio data for the single Group 3 deposit, J. Herschel, resemble those of mature low-titanium maria and are unique in this analysis. With the exceptions noted above, these observations generally confirm previous classifications by *Hawke et al.* [1989] of interdeposit compositional variation for small pyroclastic deposits. Group 1 pyroclastic deposits probably consist of feldspar-bearing mafic assemblages dominated by low-Ca orthopyroxene, and a likely explanation for their provenance is that they are mixtures of highlands-rich country rock and glass-rich juvenile material with small amounts of basaltic cap rock material. Group 2 deposits show strong affinities with mature mare deposits dominated by clinopyroxene, and they may be fragmented plug rock material, with insignificant amounts of highlands and/or juvenile materials. The single Group 3 deposit at J. Herschel has the strongest mafic absorption band and shows evidence of orthopyroxene and possibly olivine; the orthopyroxene is likely to have been emplaced as a result of erosion and entrainment of the wall rock, and the olivine may be the dominant juvenile material. It appears that the coarser spatial resolution of the Earth-based spectral data has successfully characterized the small pyroclastic deposits.

4. Juvenile Pyroclastic Materials on the Moon

Compositional data from Clementine for small lunar pyroclastic deposits generally confirm previous results and indicate that the observed range of compositions among the small deposits is consistent with an origin as products of explosive volcanic eruptions incorporating and distributing various amounts of nonjuvenile and juvenile pyroclastic material. As noted by *Head and Wilson* [1979] for small endogenic deposits at Alphonsus, the low-albedo pyroclastic deposits may consist of 50 to 100% redistributed country rock; this possibility is consistent with our observed compositional differences between the two small pyroclastic deposits at Atlas. Non-juvenile materials can consist of the complete range of lunar surface and subsurface materials in various states of maturity, with fragmented country rock (including reworked basaltic plug rock and older local mare and highlands rocks) and highlands and mare soils as the major components. Juvenile components of lunar pyroclastic eruptions are likely to be very small (submillimeter to millimeter in size [*Wilson and Head*, 1981]; ~40-μm average at Apollo 17 [*McKay and Waits*, 1978]), to include volcanic spheres (as single and compound droplets, both quenched and crystalline), crystals and crystal fragments (primarily pyroxene and olivine), and fragmented basaltic particles resulting from disruption of a foamy layer, and they may be friable or partially consolidated after deposition [e.g., *Nagle*, 1978; *Head and Wilson*, 1979]. Although known samples of small pyroclastic deposits are not recognized, a comparison of spectral data for the small deposits and those of sampled (Apollo 17/Taurus-Littrow deposit) and unsampled large deposits provides a basis for discussion of the nature of the juvenile components of both types of deposits.

As noted by *Hawke et al.* [1989], Earth-based spectral evidence for juvenile materials among the small pyroclastic deposits is strong but indirect: some component (previously referred to as a "darkening or coloring agent") is reducing the albedo of these deposits and, particularly in the case of the Group 1 deposits, broadening the long-wavelength arm of the mafic absorption feature. For Group 1 deposits, this agent has been identified as an iron-bearing pyroclastic glass [e.g.,

Hawke et al., 1989]. As noted by *McCord et al.* [1981] on the basis of Earth-based spectral data for J. Herschel, the moderate albedo and relatively strong, broad absorption band at 1 μm provide evidence that olivine is a juvenile component of this deposit. Examination of the longer-wavelength spectra from Clementine (i.e., from the near-infrared camera, or NIR spectra), especially near 2.0 μm, may allow us to constrain the possible spectral contributions of olivine versus iron-bearing pyroclastic glasses for the J. Herschel deposit. Earth-based spectral reflectance data suggest that juvenile components in the small pyroclastic deposits are most readily identified in the Group 1 and 3 deposits.

It was noted that the Apollo 17/Taurus-Littrow deposit falls far outside the range of 415/750 and 950/750 values typical of the small pyroclastic deposits (Figure 8). This fact has also been noted by *Weitz et al.* [1998], who used the Clementine UVVIS data to characterize large pyroclastic deposits at Taurus-Littrow, Sulpicius Gallus, Mare Vaporum, Rima Bode, Sinus Aestuum, Aristarchus Plateau, and Orientale. Their goal was to use spectral properties of each large deposit to infer crystallization states of pyroclastic beads and to estimate cooling rates in volcanic plumes that emplaced the deposits. Their model states that deposits with high glass concentrations were produced in volcanic plumes with low optical densities and high cooling rates, and those dominated by crystallized beads had slower cooling rates owing to higher optical densities. Although spectral contributions from nearby mare and highlands soils are acknowledged components of these deposits [*Weitz et al.*, 1998], a linear trend was observed (Figure 10) that was thought to be a mixing line between those deposits which originally had ~100% crystallized beads and those with ~100% glass beads. A Sinus Aestuum dark spot is the crystallized end-member, and Aristarchus is the glass end-member.

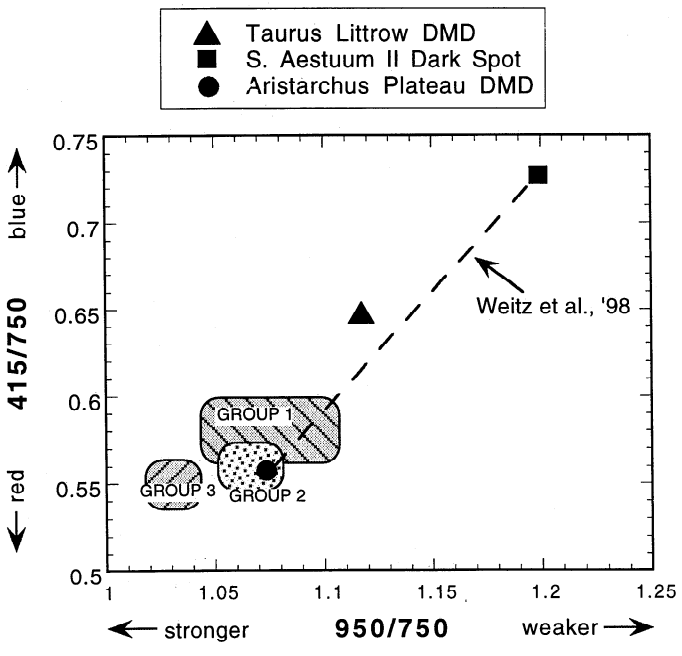

Figure 10. Clementine color ratio (415/750 versus 950/750) data for three classes of small lunar pyroclastic deposits and for three examples of large pyroclastics (Taurus-Littrow, Sinus Aestuum, and Aristarchus Plateau). The dashed line marks the possible mixing line of *Weitz et al.* [1998] between large pyroclastic deposit compositions dominated by quenched iron-bearing volcanic glasses (Aristarchus) versus crystallized beads (Sinus Aestuum).

A working assumption of *Weitz et al.* [1998] was that the titanium contents of the large pyroclastics were similar. These authors note the limitations of this assumption and point out that variations in titanium content will affect the amount of ilmenite formed in crystallized beads and thus influence the strength of the glass band absorption at 1.0 μm. It has long been recognized that several of the large pyroclastics (Taurus-Littrow, Sulpicius Gallus, Rima Bode, Mare Vaporum, and Sinus Aestuum), originally inferred to be associated with early, high-Ti volcanism in the central lunar nearside [e.g., *Pieters et al.*, 1973; *Adams et al.*, 1974; *Gaddis et al.*, 1985], probably consist of differing amounts of glass and crystallized beads such as those of Apollo 17 [*Hawke et al.*, 1990]. For these deposits, a mixing line relationship may indeed hold true. However, compositions (particularly titanium contents) of the Orientale and Aristarchus deposits are not known, and this relationship may not apply to those deposits. Although Fe^{2+}-bearing glasses in a mature lunar soil are thought to produce the observed very low albedo and strong, broad 1.0-μm band at Aristarchus, significant differences between the Aristarchus pyroclastics and the orange glasses at Apollo 17 have been noted and used to suggest that these deposits are compositionally unrelated [*Lucey et al.*, 1986; *Hawke et al.*, 1991]. In addition, substantial variation (~0.2-16 wt %) in TiO_2 among the 25 known classes of pristine lunar glasses has been observed [*Delano*, 1986].

Comparison of the Clementine color ratio data for small and large lunar pyroclastics (Figure 8) further reveals the limitations of a simple mixing relationship in explaining the observed compositional relations. Substantial overlap is observed in the color ratio data for the small and large pyroclastic deposits. As noted above, the Orientale color ratio data resemble those of the Group 1 small pyroclastic deposits. The Orientale deposit has been modeled as a large or regional lunar pyroclastic deposit by *Head et al.* [1997] and *Weitz et al.* [1998]. The unusual annular structure of the Orientale deposit is suggestive of a vulcanian eruption mechanism from a circular vent, but the large size of the Orientale pyroclastic deposit (~15,000 km^2 [*Weitz et al.*, 1998]) and its association with a central fissure vent are thought to be compatible with a long-duration, fire-fountain style of eruption. In our observations (Figure 8), the Orientale pyroclastic deposit has a higher 415/750 value than other Group 1 small pyroclastics but has a shallow mafic band similar to those of the Franklin and Alphonsus West deposits. By contrast, the large pyroclastic deposit of Aristarchus Plateau has a stronger mafic band and shows some similarity to the Group 2 small pyroclastic deposits. This overlap suggests that there may be compositional similarities between the large and small deposits in spite of their different eruption styles. The overlap may be interpreted to indicate that volcanic spheres, either quenched or crystalline, are not always the dominant juvenile component in large pyroclastic deposits; substantial highlands and mare components may also be present in some large and small pyroclastic deposits.

5. Summary and Conclusions

These analyses of the Clementine five-band spectral data for several areas on the surface of the Moon permit us to make several conclusions regarding the composition of small pyroclastic and other deposits on the Moon:

1. Mean mafic band strengths for two small pyroclastic deposits in the floor of Atlas crater are different than that of the subjacent highlands terrain, and they are different from each other. These data suggest that two distinct eruptions may have occurred from a single, possibly related vent structure and that we may be observing changes with composition through time at Atlas crater.

2. Color variations among the small pyroclastic deposits examined are consistent with those of *Hawke et al.* [1989], and our compositional interpretations are generally unchanged. Among the small pyroclastic deposits examined here, we can distinguish three compositional classes, and we see the trend of increasing mafic absorption band strength from Group 1 to Group 2 to Group 3. However, our classifications are slightly different those of *Hawke et al.* [1989], and they suggest that with additional data the three classes will aggregate into one or two groups.

3. The compositions of the small pyroclastic deposits both resemble and differ markedly from those of the larger pyroclastic deposits. Although the Apollo 17/Taurus Littrow deposit falls well beyond the three classes observed for the small deposits, the Orientale annular pyroclastic deposit resembles the Group 1 small pyroclastics and many lunar highlands units, and Aristarchus is similar to Group 2 small pyroclastic deposits and many mature lunar maria. The observed overlap in color ratio data for these large and small pyroclastic deposits suggests that simple mixing of largely volcanic bead components, either quenched or crystalline, does not adequately explain the compositional variation among lunar pyroclastic deposits. Volcanic spheres, particularly quenched iron-bearing glasses, may not always be the dominant component in some of the large pyroclastic deposits; substantial highlands and mare components may also be present in many large and small pyroclastic deposits.

4. Data for the Group 3 small pyroclastic deposit at J. Herschel support previous interpretations that it contains a juvenile component in the form of olivine [e.g., *McCord et al.*, 1981], which has acted to reduce the albedo to a moderate level and to increase the mafic band depth over the adjacent highlands terrain. Because olivine does not have an absorption feature at wavelengths longer than 1.0 μm and iron-bearing glasses do, examination of Clementine NIR data at 2.0 μm may allow us to constrain the possible spectral contributions of olivine versus iron-bearing pyroclastic glasses for this deposit.

5. Evidence for the presence of volcanic glasses in some of the small pyroclastic deposits is indirect, and it is based largely on our support for previous compositional classifications for these deposits. In the possible absence of volcanic glasses, the iron, titanium, and maturity mapping methods established by *Lucey et al.* [1998a, b] for mature mare deposits may be applicable for many of these deposits.

Acknowledgments. This paper benefitted from scientific reviews by Jeffrey R. Johnson, Jeffery Plescia, Jeffrey Gillis, and an anonymous reviewer (another Jeff?). The work was supported by NASA's Planetary Geology and Geophysics Program.

References

Adams, J.B., Visible and near-infrared diffuse reflectance spectra of pyroxenes as applied to remote sensing of solid objects in the solar system, *J. Geophys. Res., 79*, 4829-4836, 1974.

Adams, J.B., C. Pieters, and T.B. McCord, Orange glass: Evidence for regional deposits of pyroclastic origin on the Moon, *Proc. Lun. Sci. Conf. 5th*, 171-186, 1974.

Bell, P.M., H.K. Mao, and R.A. Weeks, Optical spectra and electron paramagnetic resonance of lunar and synthetic glasses: A study of the effects of controlled atmosphere, composition, and temperature, *Proc. Lun. Sci. Conf. 7th*, 2543-2559, 1976.

Blewett, D.T., B.R. Hawke, P.G. Lucey, and P.D. Spudis, A spectral survey of the Crisium basin region of the Moon, *Geophys. Res. Lett., 22*, 3059-3062, 1995a.

Blewett, D.T., B.R. Hawke, P.G. Lucey, G.J. Taylor, R. Jaumann, and P.D. Spudis, Remote sensing and geologic studies of the Schiller-Schickard region of the Moon, *J. Geophys. Res., 100*, 16,959-16,977, 1995b.

Buratti, B.J., J.K. Hillier, and M. Wang, The lunar opposition surge: Observations by Clementine, *Icarus, 124*, 490-499, 1996.

Burns, R.G., Crystal field spectra and evidence of cation ordering in olivine minerals, *Am. Mineral., 55*, 1608-1632, 1970.

Burns, R.G., *Mineralogical Applications of Crystal Field Theory*, 551 pp., Cambridge Univ. Press, New York, 1993.

Bussey, D.B.J., and P.D. Spudis, Compositional analysis of the Orientale basin using full resolution Clementine data: Some preliminary results, *Geophys. Res. Lett., 24*, 445-448, 1997.

Cloutis, E.A., and M.J. Gaffey, Pyroxene spectroscopy revisited: Spectral-compositional correlations and relationships to geothermometry, *J. Geophys. Res., 96*, 22,809-22,826, 1991.

Coombs, C.R., and B.R. Hawke, Explosive volcanism on the Moon: A review, paper presented at Kagoshima International Conference on How Volcanoes Work, IAVCEI, Kagoshima, Japan, 1988.

Coombs, C.R., B.R. Hawke, and L. Wilson, Geologic and remote sensing studies of Rima Mozart, *Proc. Lun. Planet. Sci. Conf. 18th*, 339-353, 1988.

Coombs, C.R., B.R. Hawke, P.G. Lucey, P.D. Owensby, and S.H. Zisk, The Alphonsus region: A geologic and remote sensing perspective, *Proc. Lun. Planet. Sci. Conf. 20th*, 161-174, 1990.

Delano, J.W., Pristine lunar glasses: Criteria, data, and implications, *Proc. Lun. Sci. Conf. 16th*, Part 2, *J. Geophys. Res., 91*, D201-D213, 1986.

Delano, J.W. and K. Livi, Lunar volcanic glasses and their constraints on mare petrogenesis, *Geochim. Cosmochim. Acta, 45*, 2137-2149, 1981.

Eliason, E.M., Production of Digital Image Models with the ISIS system, *Lunar Planet. Sci. XXVIII*, 331-332, 1997.

Eliason, E.M. et al., Digital processing for a global multispectral map of the Moon from the Clementine UVVIS imaging instrument, *Lunar Planet. Sci. XXX* [CD-ROM], abstract 1933, 1999.

Fischer, E.M., and C.M. Pieters, Remote determination of exposure degree and iron concentration of lunar soils using VIS-NIR spectroscopic methods, *Icarus, 111*, 475-488, 1994.

Fischer, E.M., and C.M. Pieters, Composition and exposure age of the Apollo 16 Cayley and Des Cartes regions from Clementine data: Normalizing the optical effects of space weathering, *J. Geophys. Res., 101*, 2225-2234, 1996.

Gaddis, L.R., C.M. Pieters, and B.R. Hawke, Remote sensing of lunar pyroclastic mantling deposits, *Icarus, 61*, 461-489, 1985.

Gaddis, L.R., A.S. McEwen, and T. Becker, Compositional variations on the Moon: Recalibration of Galileo solid-state imaging data for the Orientale region and far side, *J. Geophys. Res., 100*, 26,345-26,355, 1995.

Gaddis, L. et al., An overview of the Integrated Software for Imaging Spectrometers (ISIS), *Lunar Planet. Sci. XXVIII*, 387-388, 1997a.

Gaddis, L., B.R. Hawke, and M.S. Robinson, Analyses of three classes of small lunar pyroclastic deposits with Clementine data, *Lunar Planet. Sci. XXVIII*, 389-390, 1997b.

Gaddis, L., C. Rosanova, T. Hare, B.R. Hawke, C. Coombs, and M.S. Robinson, Small Lunar Pyroclastic Deposits: A new global perspective, in *Lunar Planet. Sci. XXIX* [CD-ROM], abstract 1710, 1998.

Hawke, B.R., C.R. Coombs, L.R. Gaddis, P.G. Lucey, and P.D. Owensby, Remote sensing and geologic studies of localized dark

mantle deposits on the Moon, *Proc. Lunar Planet. Sci. Conf. 19th*, 255-268, 1989.

Hawke, B.R., C.R. Coombs, and B. Clark, Ilmenite-rich pyroclastic deposits: An ideal lunar resource, *Proc. Lunar Planet. Sci. Conf. 20th*, 249-258, 1990.

Hawke, B.R., C.R. Coombs, B.A. Campbell, P.G. Lucey, C.A. Peterson, and S.H. Zisk, Remote sensing of regional pyroclastic deposits on the North Central portion of the lunar near side, *Proc. Lunar Planet. Sci. Conf. 21st*, 377-389, 1991.

Hazen, R.M., P.M. Bell, and H.K. Mao, Effects of compositional variation on absorption spectra of lunar pyroxenes, *Proc. Lunar Planet. Sci. Conf. 9th*, 2919-2934, 1978.

Head, J.W., III, Lunar dark-mantle deposits: Possible clues to the distribution of early mare deposits, *Proc. Lunar Sci. Conf. 5th*, 207-222, 1974.

Head, J.W., and L. Wilson, Alphonsus-type dark-halo craters: Morphology, morphometry, and eruption conditions, *Proc. Lunar Planet. Sci. Conf. 10th*, 2861-2897, 1979.

Head, J.W. and L. Wilson, Lunar mare volcanism: Stratigraphy, eruption conditions, and the evolution of secondary crusts, *Geochim. Cosmochim. Acta, 56*, 2155-2175, 1992.

Head, J.W., L. Wilson, and C. Weitz, The dark ring in southwestern lunar Orientale basin: Origin as a single pyroclastic eruption, *Lunar Planet. Sci. XXVIII*, 543-544, 1997.

Heiken, G.H., D.S. McKay, and R.W. Brown, Lunar deposits of possible pyroclastic origin, *Geochim. Cosmochim. Acta*, *38*, 1703-1718, 1974.

Johnson, J.R., S.M. Larson, and R.B. Singer, Remote sensing of potential lunar resources, 1. Near-side compositional properties, *J. Geophys. Res., 96*, 18,861-18,882, 1991.

Jolliff, B.L., Clementine UVVIS multispectral data and the Apollo 17 landing site: What can we tell and how well?, *J. Geophys. Res., 104*, 14,123-14,148, 1999.

Li, L., J. F. Mustard, and C. M. Pieters, The effects of scattered light in the Clementine UV-VIS camera on mixture analysis, in *Lunar Planet. Sci. XXX* [CD-ROM], abstract 1866, 1999.

Lucchitta, B.K., Geologic setting of the dark mantling material in the Taurus-Littrow region of the moon, in *Apollo 17 Preliminary Science Report, NASA SP-330*, 29-13 to 29-25, 1973.

Lucey, P.G., B.R. Hawke. C.M. Pieters, J.W. Head, and T.B. McCord, A compositional study of the Aristarchus region of the Moon using near-infrared reflectance spectroscopy, *J. Geophys. Res.*, *91*, 344-354, 1986.

Lucey, P.G., P.D. Spudis, M. Zuber, D. Smith, and E. Malaret, Topographic-compositional units on the Moon and the early evolution of the lunar crust, *Science*, *266*, 1855-1858, 1994.

Lucey, P.G., D.T. Blewett, and B.R. Hawke, Mapping the FeO and TiO_2 content of the lunar surface with multispectral imagery, *J. Geophys. Res.*, *103*, 3679-3699, 1998a.

Lucey, P.G., G.J. Taylor, and B.R. Hawke, Global imaging of maturity: Results from Clementine and lunar sample studies, in *Lunar Planet. Sci. XXIX* [CD-ROM], abstract 1356, 1998b.

McCord, T.B., R.M. Clark, B.R. Hawke, L.A. McFadden, P.D. Owensby, C.M. Pieters, and J.B. Adams, Moon: Near-infrared spectral reflectance, A first good look, *J. Geophys. Res.*, *86*, 10,883-10,892, 1981.

McEwen, A.S., Photometric functions for photoclinometry and other applications, *Icarus*, *92*, 298-311, 1991.

McEwen, A.S., A precise lunar photometric function, *Lunar Planet. Sci. XXVII*, 841-842, 1996.

McEwen, A.S., and M.S. Robinson, Mapping the Moon by Clementine, *Adv. Space Res.*, 19(10), 1523-1533, 1997.

McEwen, A.S., E. Eliason, P. Lucey, E. Malaret, C. Pieters, M. Robinson, and T. Sucharski, Summary of radiometric calibration and photometric normalization steps for the Clementine UVVIS images, *Lunar Planet. Sci. XXIX* [CD-ROM], abstract 1466, 1998.

McKay, D. and G. Waits, Grain size distribution of samples from core 74001 and 74002, *Lunar Planet. Sci. IX*, 723-725, 1978.

Morrison, D.A. and D. Ben J. Bussey, The Apollo and Korolev basins and the stratigraphy of the lunar crust, *Lunar Planet. Sci. XXVIII*, abstract 1501, 1997.

Mustard, J.F., L. Li, and G. He, Nonlinear spectral mixture modeling of lunar multispectral data: Implications for lateral transport, *J. Geophys. Res.*, *103*, 19,419-19,425, 1998.

Nagle, J. S., A comparison of a lunar and a terrestrial volcanic section, *Proc. Lunar Planet. Sci. Conf. 9th*, 1509-1526, 1978.

Nozette, S. et al., The Clementine Mission to the Moon: Scientific overview, *Science*, *266*, 1835-1839, 1994.

Papike, J.J., G. Ryder, and C.K. Shearer, Lunar samples, in Planetary Materials (chap. 5), *Reviews in Mineralogy*, *36*, 5.1-5.234, 1998.

Pieters, C.M., Composition of the lunar highland crust from near-infrared spectroscopy, *Rev. Geophys., 24*, 557-578, 1986.

Pieters, C.M., and P.A.J. Englert (eds.), *Remote Geochemical Analysis: Elemental and Mineralogical Composition*, 594 pp., Cambridge Univ. Press, New York, 1993.

Pieters, C.M., T.B. McCord, S.H. Zisk, and J.B. Adams, Lunar black spots and the nature of the Apollo 17 landing area, *J. Geophys. Res.*, *78*, 5867-5875, 1973.

Pieters, C.M., T.B. McCord, Charette, M.P., and J.B. Adams, Lunar surface: Identification of the dark mantling material in the Apollo 17 soil samples, *Science*, *183*, 1191-1194, 1974.

Pieters, C. M. et al., Crustal diversity of the Moon: Compositional analyses of Galileo SSI data, *J. Geophys. Res.*, *98*, 17,127-17,148, 1993.

Robinson, M.S., E.M. Shoemaker, and B. R. Hawke, Spectral heterogeneity of lunar local dark mantle deposits, *Lunar Planet. Sci. XXVII*, 1087-1088, 1996.

Robinson, M.S., A. S. McEwen, E. M. Eliason, E. M. Lee, E. Malaret, P. Lucey, Clementine UVVIS Global Mosaic: A new tool for understanding the lunar crust, *Lunar Planet. Sci. XXX* [CD-ROM], abstract 1931, 1999.

Rosanova, C., L. Gaddis, T. M. Hare, C. Coombs, B. R. Hawke, and M. S. Robinson, Characterization of "new" pyroclastic deposits on the Moon using Clementine data, in *Lunar Planet. Sci. XXIX* [CD-ROM], abstract 1807, 1998.

Shearer, C.K., and J.J. Papike, Basaltic magmatism on the Moon: A perspective from volcanic picritic glass beads, *Geochim. Cosmochim. Acta*, *57*, 4785-4812, 1993.

Shoemaker, E.M., M.S. Robinson, and E. M. Eliason, The South Pole region of the Moon as seen by Clementine, *Science*, *266*, 1851-1854, 1994.

Spudis, P.D., Young dark mantle deposits on the Moon, *NASA Tech. Memo. 4210*, 406-407, 1989.

Sunshine, J.M., and C.M. Pieters, Estimating modal abundances from the spectra of natural and laboratory pyroxene mixtures using the modified Gaussian model, *J. Geophys. Res., 98*, 9075-9087, 1993.

Tompkins, S., and C.M. Pieters, Mineralogy of the lunar crust: Results from Clementine, *Meteorit. Planet. Sci.*, *34*, 25-41, 1999.

Torson, J. and K. Becker, ISIS - A software architecture for processing planetary images, *Lunar Planet. Sci. XXVIII*, 1443-1444, 1997.

Weitz, C.A., J.W. Head III, and C.M. Pieters, Lunar regional dark mantle deposits: Geologic, multispectral, and modeling studies, *J. Geophys. Res.*, *103*, 22,725-22,759, 1998.

Wilhelms, D., The geologic history of the Moon, *U.S. Geol. Surv. Prof. Pap. 1348*, 544 pp., 1987.

Wilson, L.W., and J.W. Head, III, Ascent and eruption of basaltic magma on the Earth and Moon, *J. Geophys. Res., 86*, 2971-3001,1981.

Yingst, R.A., and J.W. Head, III, Characteristics of lunar mare deposits in Smythii and Marginis basins: Implications for magma transport mechanisms, *J. Geophys. Res., 103*, 11135-11158, 1998.

C. Coombs, Department of Geology, College of Charleston, Charleston, SC 29424.

L.R. Gaddis, Astrogeology Program, U.S. Geological Survey, 2255 N. Gemini Drive, Flagstaff, AZ 86001. (lgaddis@flagmail.wr.usgs.gov).

B.R. Hawke, PGD/SOEST, University of Hawaii, 2525 Correa Road, Honolulu, HI 96822.

M.S. Robinson, Department of Geological Sciences, Northwestern University, Evanston, IL 60208.

(Received April 20, 1999; revised August 11, 1999;
accepted August 13, 1999.)